STEADY-STATE HIGH PRESSURE LOX/H_2 ROCKET ENGINE COMBUSTION

Joshua J. Smith, Martin Bechle, Dmitri Suslov, Michael Oschwald, Oskar Haidn
German Aerospace Centre DLR – Institute of Space Propulsion, Hardthausen, Germany

Gerald Schneider
School of Mechanical Engineering, University of Adelaide, Australia

Introduction

Understanding injection and combustion phenomena at elevated pressures in liquid rocket engines (LRE's) is necessary to promote ongoing performance enhancements for existing and future applications. Exhaustive experimental testing of liquid rocket engines under representative operating conditions is prohibitively expensive and will eventually be replaced or at least reduced by advanced numerical modelling techniques. Before this can occur, the significant progresses made in high-pressure theoretical and numerical studies [1-3] require validation from well-defined, representative experimental databases.

Recent observations of high pressure injection of O_2/H_2 under reacting [4-10] and various simulants under non-reacting conditions [11-16] have highlighted significant physical disparities between sub- and supercritical injection and atomisation regimes. Strong influences are primarily owing to strong thermodynamic gradients and non-idealities experienced under near critical and supercritical pressure conditions. Further details on supercritical fluid thermodynamic and transport properties are provided in the references.

Results and outcomes from previous experimental and numerical studies have motivated further investigations with the application of time-resolved optical diagnostics to an optically accessible, single shear coaxially injected high pressure LOx/H_2 thrust chamber with an advanced and highly accurate measurement system. The test specimen is operated at the P8 test facility located at the German Aerospace Centre DLR Institute of Space Propulsion with a description of the facility presented in [17]. Hardware, measurement system and diagnostics are described in detail in [18]. Brief details of the optical diagnostics system and hardware are provided in the following sections.

Observations and results from a broad range of combustion tests are presented focussing on the influence of relative propellant velocity ratio and oxidiser reduced pressure ($P_r=P_{ch}/P_{O2crit}$) on steady-state combustion noise, propellant flow field and flame emission. The influence of injection conditions on combustion response and near injector flame emission is also detailed. Transient processes are not discussed here for the sake of brevity but can be located elsewhere [18].

Motivation

Propellants injected into liquid rocket thrust chambers at supercritical conditions behave as dense gases with gas-like diffusivities. Large thermodynamic gradients exist near the critical point with properties such as specific heat (c_p) and isothermal compressibility (k_T) peaking dramatically at the critical point, warranting evaluation of real fluid properties when considering supercritical or near critical conditions (see Figure 1). All fluid properties and operating conditions presented here are derived based upon a Modified Benedict-Webb-Rubin equation of state [19].

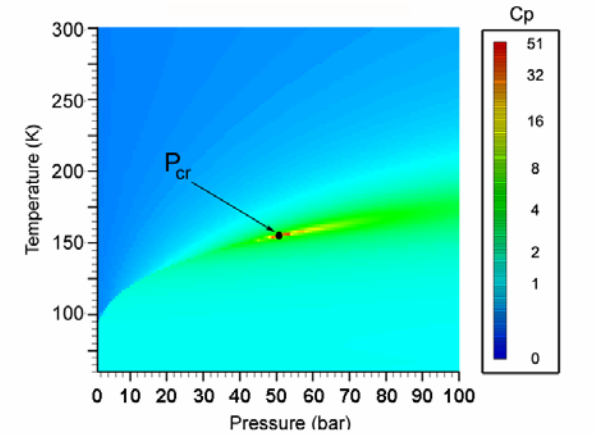

Figure 1 – Specific Heat (c_p) of O_2. (calculated based on a MBWR equation of state)

Limited data-sets exist for high pressure LOx/H_2 combustion and empirically derived correlations for low-pressure (subcritical) injection and combustion phenomena cannot be directly extrapolated to trans- or supercritical regimes. The Weber number (*We*) is undefined above a reduced pressure of unity due to the absence of surface tension and thus existing correlations based on *We* cannot be applied. Other empirically derived correlations such as intact core length (L_c) fall short by up to 3 orders of magnitude and other non-dimensional numbers frequently employed to characterise subcritical coaxial sprays in reacting and non-reacting environments have not been proven to have similar influences on flow field characteristics at high pressures (i.e. Propellant momentum flux ratio *J* and injection velocity ratio v_R).

Stability rating of LOx/H_2 rocket engines has been comprehensively investigated in the past however data has been typically published only from subcritical pressure test conditions. Stability rating data for elevated pressure (supercritical) LOx/H_2 combustion cannot be obtained or located by the author, which poses questions as to the validity of directly extrapolating low pressure stability limits to high pressure operating conditions.

Aims

This work aims at providing a parametric study of various operating conditions and their influences on combustion response, combustion efficiency and flame and flow field stability under stead-state operating conditions. A data base with well defined boundary and representative operating conditions would assist in the validation of existing and future numerical models developed for high pressure combustion. Combined numerical and experimental efforts will advance the current understanding of high pressure injection and combustion and complement the existing foundation of knowledge in this field.

Hardware and Operating Conditions

A high-pressure windowed combustion chamber is used for the visualisation component of the experimental campaign with details outlined in [7]. An advanced measurement system has been developed comprising high frequency static and dynamic pressure, mass flow rate and temperatures measurements throughout the test specimen. Details can be found in [18]. A range of coaxial injector elements were used in the test series with various geometries. This was necessary to achieve different relative propellant injection velocities at constant injection temperature conditions. Typically, LOx post diameter and thickness were maintained constant at 4mm and 0.3mm respectively whilst H_2 injection diameter was modified. Details can be located elsewhere [18].

An operating sequence was developed to achieve three pressure levels during a single test. This was accomplished through propellant flow rate regulation at a constant oxidiser-fuel ratio (R_{OF}). Each pressure level is designated Phase 1, 2 and 3 for $P_r > 1$, $P_r \sim 1$, and $P_r < 1$ respectively. Steady state operation is defined when all injection conditions are constant (i.e. chamber pressure, propellant flow rates, injection temperatures etc. Typical time-

pressure and temperature traces are shown in Figures 2 and 3.

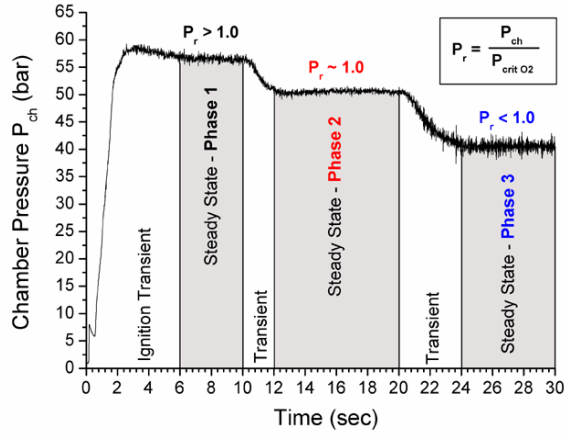

Figure 2 – Chamber pressure trace indicating 3 operating phases (from [10])

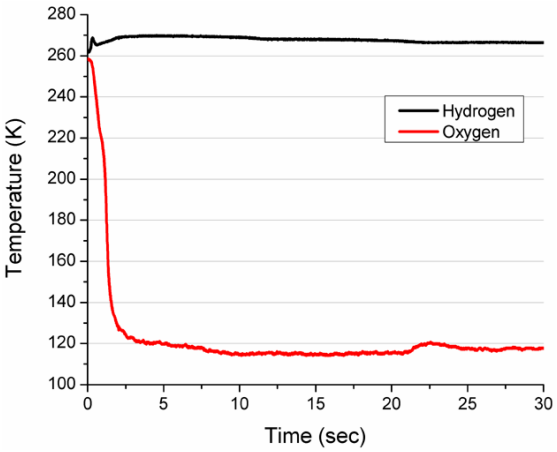

Figure 3 – Constant propellant injection temperatures recorded throughout a single test

Oxygen injection temperatures were maintained relatively constant throughout all tests whereas two distinct H_2 temperature ranges were thoroughly investigated ($130K<T_{H2}<150K$ and $230<T_{H2}<270K$). Figure 4 represents the operating conditions in terms of injection velocity ratio v_R as a function of reduced chamber pressure for all three operating phases. Values presented are based on the thermophysical properties calculated using the MBWR equation of state combined with the measurement data recorded throughout operation of the test specimen. All thermocouples and propellant mass flow meters are are calibrated with a maximum error of <1% and 4% respectively. Further details can be located in [18]. Momentum flux ratio J has shown to be strongly related to v_R over the range of conditions investigated (i.e. see reference [18]). Due to this, only v_R effects are investigated here although comparison with J would yield similar results.

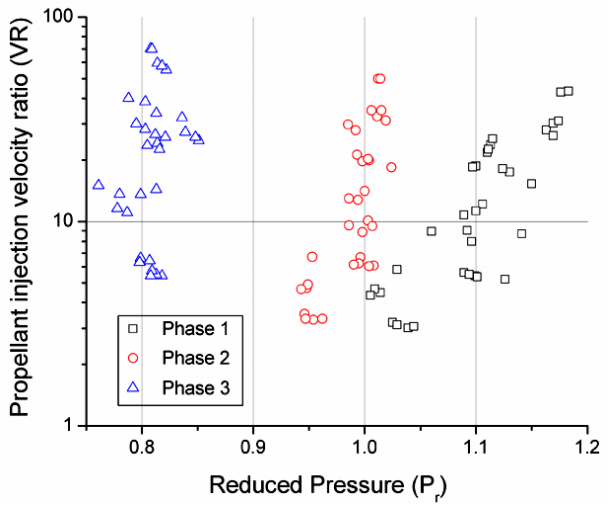

Figure 4 – Operating conditions in terms of injection velocity ratio and combustion chamber reduced pressure

Optical Diagnostics

High sound pressure and vibration levels combined with space restrictions led to the development of a range of unique optical diagnostics setups to observe the near injector flow field and combustion zone. A schematic of the setup is represented by Figure 5.

A range of camera systems were operated remotely to observe the OH radical chemiluminescence, spontaneous H_2O emission and the propellant flow-field behaviour using a high-speed backlit shadowgraph setup. The optical diagnostic system was arranged around the thrust chamber as shown in Figure 5 with optical accessibility via 3 quartz glass windows.

Spontaneous OH emission was recorded from the near injector region using an image intensified Photron Ultima i2 SE fastcam with a 4µs gated shutter and a narrowband optical filter for transmission of the OH radical. The acquisition frequency used was f = 9kHz with a 128x256 pixel image resolution. High speed diagnostics were implemented to ensure high temporal resolution enabling observation of flow-field and combustion dynamics. Flame dynamics is not presented due to paper length constraints however the analysis detailed here utilises the fact that large image sets are obtained providing improved statistical confidence. The system was operated in burst mode capturing

256 frames every 0.5 seconds to avoid image biasing which could occur should the system be operated in continuous mode. Further details of the other cameras used can be found in reference [10].

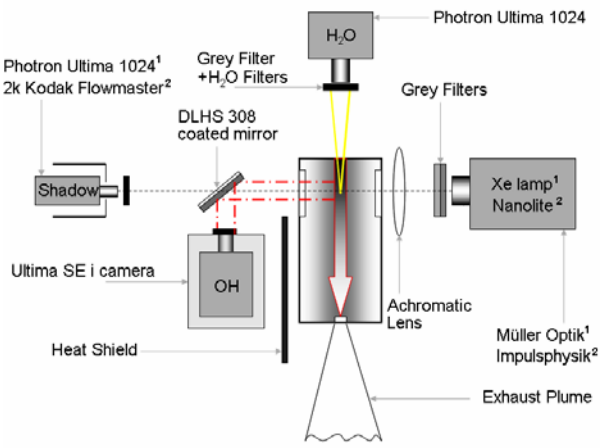

Figure 5 – Optical diagnostics schematic

Analysis Techniques

A range of data reduction and image processing techniques are applied to assess the combustor response and flame stability over the range of conditions examined. Other image processing techniques are omitted for succinctness and are detailed elsewhere in reference [18]

- Combustion efficiency (η) is calculated based on standardised theory [20] and presented as a function of P_r.
- Shadowgraph and flame emission images are time-averaged to provide an indication of flow-field behaviour as a function of P_r and injection conditions.
- Dynamic pressure data is assessed through examination of peak-to-peak pressure values to understand combustion response to various operating conditions.
- A normalised emission intensity threshold technique is applied to assess the axial variation of flame intensity as a function of injection conditions such as v_R and P_r.
- Mean radical emission intensity is investigated as a function of injection conditions such as v_R and P_r.

Details of the techniques listed are not detailed here but can be found in reference [18].

Results

The range of diagnostics applied to the test specimen has highlighted a significant difference between steady state combustion regimes at elevated pressures. At the nominal chamber pressure between P_{ch} = 51 and 60 bar, condensation of H_2O was consistently observed to reduce emission intensity through scattering and absorption effects. At 60 bar, the vapour temperature of water is around T_{vap} ~ 594K. Decreasing H_2 injection temperature and increasing chamber pressure both proved detrimental to visualisation of the near injector region due to an increase in condensation. At near critical and subcritical chamber pressures, the condensation was not observed. Temperature measurements in the combustion chamber at similar conditions have indicated that such low temperatures can indeed exist supporting the theory of condensed water shrouding the flame and inhibiting visual access [7]. Figure 6 illustrates the effect of the reduced emission intensity at high pressure with a series of time averaged OH emission images. This observation is further supported by spectroscopic measurement data [18].

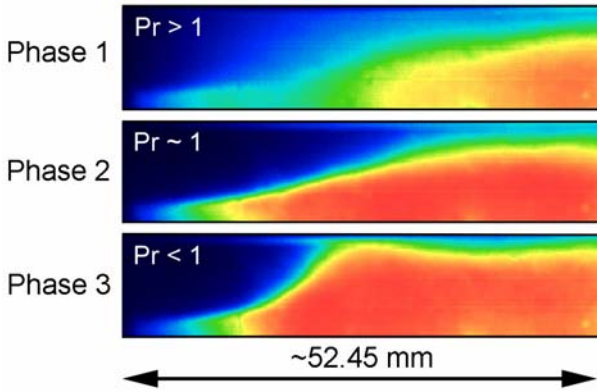

Figure 6 – Time averaged OH emission images highlighting lower emission intensity during Phase 1

The combustion efficiency η also indicates an obvious distinction between operating regimes. Figure 7 highlights a strong relation between η and v_R. For reduced pressure conditions less than unity, there appears to be a linear relationship between η and v_R. At P_r equal to and greater than one, a very strong influence of v_R on η is observed for $v_R < 10$ and $v_R < 20$ respectively. Above these v_R values, the rate of change in η is comparable to that for $P_r < 1$ (Phase 3). This dissimilarity between phases supports previous observations of entirely different atomisation and mixing regimes between subcritical, and supercritical pressure conditions [4,9,12-16].

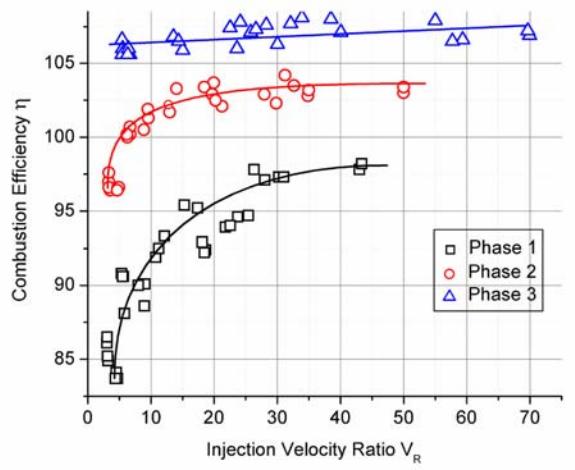

Figure 7 – Combustion efficiency as a function of injection velocity ratio and operating phase (from [10]).

The near injector zone flow-field and combustion zone exhibits an inherent unsteadiness which is clearly and consistently observed in the plethora of emission and shadowgraph images recorded. Figure 8 illustrates this unsteadiness with a series of spontaneous and time-averaged shadowgraph images captured from all phases during a single test. The steadiness at increased pressure is apparent and was consistently observed during tests where the shadowgraph setup was successfully implemented.

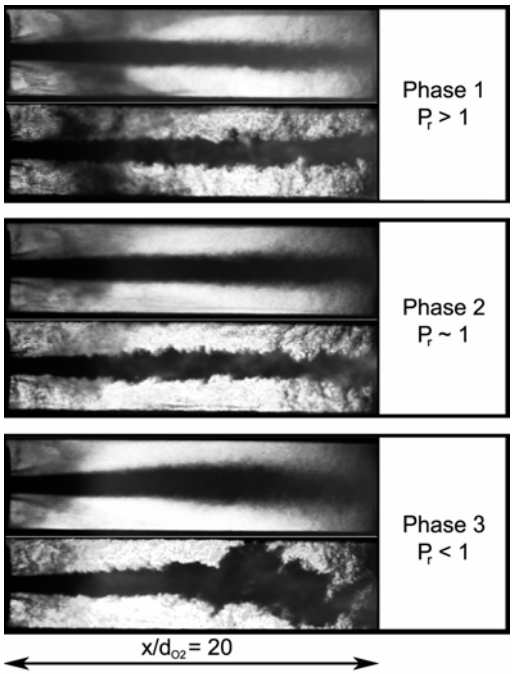

Figure 8 – Time-averaged and instantaneous shadowgraph emission images from all operating phases.

Dynamic pressure data recorded throughout steady-state chamber operation is examined. The technique calculates the variance of the peak-to-peak pressure values whereby data is assessed based on measured combustion chamber pressure amplitudes (P_i) relative to mean combustion chamber pressure $\overline{P}_{ch}$ as follows;

$$P_{p-p}^2 = \frac{1}{(N-1)} \sum_{i=1}^{N} (P_i - \overline{P}_{ch})^2$$

$\overline{P}_{ch}$ is based on a running average from three consecutive static chamber pressure values. Steady state data from a typical test is presented in Figure 9 that clearly exhibits an increase of peak-to-peak amplitudes ($P_{p\text{-}p}$) at subcritical pressures. This finding is consistently observed over the test range considered.

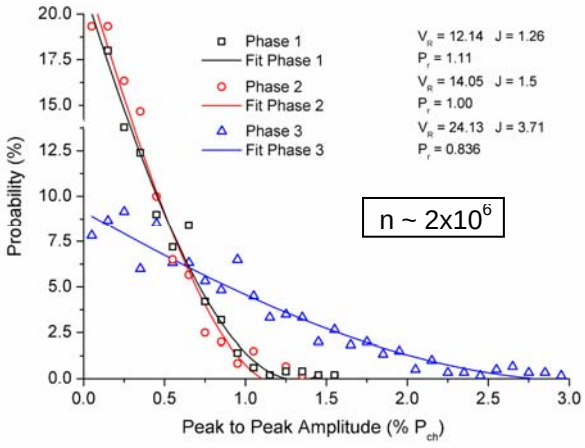

Figure 9 – Peak-to-peak amplitudes of combustion chamber pressure for 3 operating phases recorded during a single test

The flame is assessed through the implementation of an array of image processing techniques which can are detailed in reference [18]. Two techniques are presented here which examine the global flame emission intensity and axial emission position analysis during stationary operating conditions.

Figure 10 represents the normalised OH emission intensity I_{OH} calculated for a range of tests and corresponding operating phases at conditions where $146<T_{H2}<164$K. Each point represents a mean emission intensity value calculated from 256 separate images. It is evident from Figure 10 that the flame OH emission intensity is strongly influenced by the injection velocity ratio at reduced pressures greater than or equal to unity. Under conditions where $P_r < 1$, a linear relationship exists between v_R

and I_{OH}. This observation is consistent with the velocity ratio effect on combustion efficiency (Figure 7). This leads us to the intuitive fact that the flame emission intensity I_{OH} is clearly related to the combustion efficiency η.

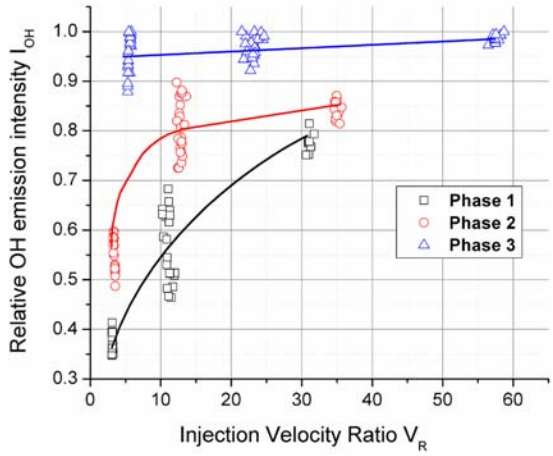

Figure 10 – Flame relative OH emission intensity as a function of injection velocity ratio and operating phase. Data plotted from tests with 146K < T_{H2} < 164K and 110K < T_{O2} < 125K (from [18])

The flame is further assessed based on the mean axial position of a relative OH emission intensity gradient as a function of injection conditions. A series of emission intensity *threshold* values are prescribed to large series' of normalised OH emission images (i.e. $0.1\bar{I}$,$0.15\bar{I}$,$0.2\bar{I}$ etc.) and the downstream axial positions are recorded. The mean of these axial positions is then presented.

Comparison of the mean emission intensity positions between operating phases is portrayed by Figure 11 which clearly illustrates the effect of injection velocity ratio on the combustion field. The prescribed mean flame threshold position tends to move further downstream with reduced relative propellant velocities. Once again, a distinct difference is observed between operating regimes. A linear relation is obvious between mean downstream flame threshold position and v_R for P_r < 1. However, a very strong influence of v_R on threshold position is visible for v_R < 10 at near critical pressure conditions (P_r ~ 1).

This observation and is consistent over a series of steady state tests whereby hydrogen injection temperature was between 222<T_{H2}<251K. Phase 1 data is not included due to the aforementioned water condensation falsifying the results and some Phase 3 data is omitted due to the occurrence combustion instability [18].

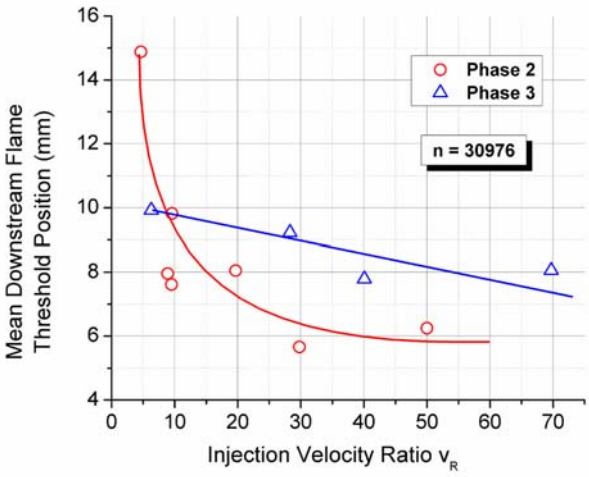

Figure 11 – Mean downstream flame threshold position as a function of injection velocity ratio. Note Phase 1 data is omitted due to water condensation. Some Phase 3 data is also absent due to the occurrence of combustion instability. Tests with 222K<T_{H2} < 251K.

Concluding Remarks

A sub-scale H_2/O_2 coaxially injected model combustor with optical access has been operated at a range of steady-state conditions representative of real liquid rocket engines. A range of injection velocity ratios and chamber pressures are investigated by interchanging injector geometries and regulating propellant flow-rates at constant R_{OF}.

Measurement system data has indicated a significant difference exists when operating the thrust chamber at pressures below, near and above the thermodynamic critical pressure of oxygen. Both the combustion efficiency estimation (η) and the variance calculation of peak to-peak dynamic pressure data (P^2_{p-p}) have consistently highlighted dissimilar behaviour which can be attributed to an entirely different atomisation and mixing phenomenon at conditions where reduced pressure (with respect to O_2) is greater than or equal to one.

Application of high-speed time resolved diagnostics has provided further support through flow-field visualisation and analysis of flame emission data. The results highlight trends very similar to those observed by the measurement system data. It must be emphasised that all four independent analysis techniques have exhibited a strong influence of

injection velocity ratio v_R on the overall combustor response and localised, near injector flame behaviour. All techniques concur that reduced pressure also plays a critical role and further influences the effects relative propellant velocities have on mixing, atomisation and flow field evolution. Examination of the near injector field has proven to be an effective method of evaluating the global performance of a liquid rocket engine thrust chamber.

Such observations highlight the need for further experimental investigations to provide additional information and enhance the current understanding of high pressure combustion.

References

[1] Oefelein, J. Thermo-physical Characteristics of Shear-Coaxial LOx-H_2 Flames at Supercritical Pressure, *Proc. Combust. Inst.* Chicago, 2004.

[2] Okongo, N., Harstad, K.G., and Bellan, J. Direct Numerical Simulation of O2/H2 Temporal Mixing Layers Under Supercritical Conditions, *AIAA Journal* Vol. 40, No. 5, pp 914-926, 2002.

[3] Yang, V. Modelling of Supercritical Vaporization, Mixing and Combustion Processes in Liquid–Fueled Propulsion Systems, *Proc. Combust. Inst.* Vol. 28, pp 925-942, 2000.

[4] Mayer, W. and Tamura, H. Propellant Injection in a Liquid Oxygen/Gaseous Hydrogen Rocket Engine. *Journal of Propulsion and Power*. Vol. 12, No. 6, pp. 1137-1147, 1996.

[5] Mayer, W.O.H., Schik, A.H.A., Vielle, B., Chauveau, C., Gökalp, I., Talley., D.G. Atomization and Breakup of Cryogenic Propellants under High Pressure Subcritical and Supercritical Conditions. *Journal of Propulsion and Power*, Vol. 14, No.5, 1998, pp. 835-842.

[6] Juniper, M., Tripathi, A., Scouflaire, P., Rolon, C., Candel, S., *The Structure of Cryogenic Flames at Subcritical and Supercritical Pressures*. In: *Combustion dans les Moteurs Fusées,* CNES, 2001.

[7] Smith, J.J., Klimenko, D., Clauss, W., and Mayer, W. Supercritical LOX/Hydrogen Rocket Combustion Investigations Using Optical Diagnostics. *38th AIAA/ASME/SAE/ASEE Joint Propulsion Conference and Exhibit*, Paper 2002-4033, 2002.

[8] Ivancic, B., and Mayer, W. Time- and Length Scales of Combustion in Liquid Rocket Thrust Chambers, *Journal of Propulsion and Power*, Vol. 18, No.2, pp 247-254, 2002.

[9] Mayer, W., and Smith, J.J. *Fundamentals of Supercritical Mixing and Combustion of Cryogenic Propellants*, In: Yang, V., Habiballah, M., and Popp, M., *Liquid Rocket Thrust Chambers:Aspects of Modeling, Analysis and Design*, AIAA Progress in Aeronautics and Astronautics, 2004.

[10] Smith, J. J., Bechle, M., Suslov, D., Oschwald, M., Haidn, O. J., Schneider, G. M. High Pressure LOX/H_2 Combustion and Flame Dynamics-Preliminary Results, *38th AIAA/ASME/SAE/ASEE Joint Propulsion Conference and Exhibit*, Paper 2004-3376, 2004.

[11] Oschwald, M., and Schik, A. Supercritical nitrogen free jet investigated by spontaneous Raman scattering, *Experiments in Fluids*, Vol. 27, pp. 497-506, 1999.

[12] Chehroudi, B., and Talley, D. Fractal Geometry of a Cryogenic Nitrogen Jet Injected into Sub- and Supercritical Conditions, *Atomization and Sprays*, Vol. 14, pp 81-91, 2004.

[13] Branam, R., and Mayer, W., Characterization of Cryogenic Injection at Supercritical Pressure, *Journal of Propulsion and Power*, Vol. 19, No.3, pp. 342-355, 2003.

[14] Chehroudi, B., Talley, D., and Coy, E. Visual Characteristics and Initial Growth Rates of Round Cryogenic Jets at Subcritical and Supercritical Pressures, *Physics of Fluids,* Vol. 14, No. 2, pp 850-861, 2002.

[15] Mayer W., Telaar, J,, Branam, R., and Hussong, J. Raman Measurements of Cryogenic Injection at Supercritical Pressure, *Heat and Mass Transfer*, Vol. 39, pp 709 – 719, 2003.

[16] Chehroudi, B., Talley, D. Fractal Geometry of a Cryogenic Nitrogen Round Jet Injected into Sub- and Supercritical Conditions, *Atomization and Sprays*, Vol. 14, pp 81-91, 2004.

[17] Koschel, W., and Haidn, O.J. P8- The New French/German Test Facility for H_2/O_2 High Pressure Rocket Engine Combustion Research, *International Journal of Hydrogen Energy*, Vol. 23, No. 8, pp 683-694, 1998.

[18] Smith, J.J. High Pressure LOx/H2 rocket engine combustion, Ph.D dissertation, University of Adelaide, 2005 (pending submission).

[19] Schmidt, R., Wagner, W. A new form of the equation of state for pure substances and its application to oxygen, *Fluid Phase Equilibria* Vol. 19, pp 175-200, 1985.

[20] Gordon S., and McBride, B.J. Computer Program for Calculation of Complex Equilibrium Compositions and Applications, NASA, 1994.